Cancellation of Spiral Wave and Spatiotemporal Chaos by Synchronization of Network

Chengye Zou, Xingyuan Wang, Haifeng Li, Chun Huang

Abstract—**In cardiac clinical trials, appearance of spiral waves in myocardium electrical signal is associated with the arrhythmia and tachycardia. Spatiotemporal chaos generates form breakup of spiral waves, and may lead to ventricular fibrillation. Therefore, cancellation of spiral wave and spatiotemporal chaos can avoid the emergence of arrhythmia, tachycardia and ventricular fibrillation. Kinetic behavior of cardiac myocytes is well described by Fitzhugh–Nagumo model. In this paper, Fitzhugh–Nagumo model as node for a network. Spiral waves or the spatiotemporal chaos of a nodes have been canceled by bidirectional feedback, then spiral waves or the spatiotemporal chaos of the other node is suppressed through synchronization of network. Numerical simulation results demonstrate that proposed method can eliminate spiral wave and spatiotemporal chaos of the network effectively. Compared with previous synchronization tactics such as active-passive decomposition method and Lyapunov exponent method, our proposed method has better synchronization performance within network.**

Index Terms—**cardiac myocytes, network, synchronization, Fitzhugh-Nagumo model**

I. Introduction

The investigation of pattern is improved quickly throughout the development of the nonlinear dynamics in recent years. Pattern originates from dynamic process of location and interaction of diffusion, it can be found in biological, physical, and chemical systems [1-10]. For instance, cardiac clinical trials indicate that arrhythmia and tachycardia are corresponding to the spiral waves in myocardium electrical signal. The breakup of spiral waves will develop into spatiotemporal chaos, which is associated with ventricular fibrillation, and harms people's life extremely [11-17], therefore how to eliminate spiral waves and spatiotemporal chaos is important to watch. At present, the main cardiac therapies are medicines and high voltage defibrillator, however, drugs have toxic side effects, and high voltage signal is very dangerous to stimulate and inspire the heart.

This research is supported by the National Natural Science Foundation of China (No: 61672124), the Password Theory Project of the 13th Five-Year Plan National Cryptography Development Fund (No: MMJJ20170203), and The Science and Technology Project of Henan Province (No: 202102310202).

Chengye Zou is a lecturer of School of Mathematics and Statistics, Anyang Normal University, Anyang 455000, China (e-mail: zouchengye0717@163.com).

Xingyuan Wang is a professor of School of Information Science and Technology, Dalian Maritime University, Dalian 116026, China (e-mail: xywang@dlmu.edu.cn).

Haifeng Li (corresponding author) is a doctoral candidate of School of Software, Dalian University of Technology, Dalian 116024, China (e-mail: lihaifeng8848@mail.dlut.edu.cn).

Chun Huang (corresponding author) is an associate professor of College of Electrical and Electronic Engineering, Zhengzhou University of Light Industry, Zhengzhou, 450002, China (e-mail: huangchunzzuli@yeah.net).

It is exciting that spiral waves and spatiotemporal chaos can be eliminated through the dynamical characters of spiral waves in cardiac tissues [18-24]. Xu eliminated the spiral waves in cardiac tissue by hybrid strategy [25], Guo studied the elimination of spiral turbulence based on feedback method [26], Yuan controlled the spiral waves by periodic pulses [27]. Li investigated the controlled spiral waves and spatiotemporal chaos by dislocation coupling method [28].

With the deepening of research, it is found that, spiral waves and spatiotemporal chaos in many practical systems are not isolated and single, they have complex interconnections between each other and can form a huge complex network. For example, in a neuronal network, elimination of spiral wave and spatiotemporal chaos in the whole network can be realized through synchronization [29]. Spiral wave and turbulence of Fitzhugh–Nagumo system are transmit by synchronization in network [29, 30]. In myocardium, multiple spiral waves and spatiotemporal chaos may appear, when heart is abnormal, thus spiral waves and spatiotemporal chaos are regarded as nodes of network. Spiral wave and turbulence of are eliminated through synchronization of network [31].

In this work, we propose a new method to eliminate multiple spiral wave and spatiotemporal chaos of myocardium by synchronization of network. Compared with [29, 30], we realize synchronization of network is based on the assignment coupling strengths without controllers, but [29, 30] achieve synchronization of network by controllers. Compared with [31], the first node of spiral wave and spatiotemporal chaos is canceled by bidirectional feedback, the other spiral wave and spatiotemporal chaos is canceled based on the synchronization of network, but spiral wave and spatiotemporal chaos of the first node is canceled by external signal in [31]. Simulation results show the effectiveness and advantage of the proposed method. In the section of analysis and discussion, the synchronization performance of proposed method is better than active-passive decomposition method and Lyapunov exponent method.

II. Mechanism of Elimination of Spiral Waves and Spatiotemporal Chaos

A. Mechanism of suppression of spiral waves and spatiotemporal chaos

The Fitzhugh–Nagumo equation with two variables is one of the typical theoretical models to describe the spiral wave and turbulence of cardiomyocyte, which is depicted as [32]

$$\begin{cases}\frac{\partial u(\gamma,t)}{\partial t}=\varepsilon^{-1}u(\gamma,t)(1-u(\gamma,t))\left(u(\gamma,t)-\frac{v(\gamma,t)+b}{a}\right)\\ \qquad +D\nabla^2u(\gamma,t)\\ \frac{\partial v(\gamma,t)}{\partial t}=f(u(\gamma,t))-v(\gamma,t)\end{cases} \tag{1}$$

$$f(u(\gamma,t))=\begin{cases}0 & 0\le u(\gamma,t)<1/3\\ 1-cu(u-1)^2 & \frac{1}{3}\le u(\gamma,t)<1\\ 1 & u(\gamma,t)\ge 1\end{cases} \tag{2}$$

where $u(\gamma,t)$ and $v(\gamma,t)$ represents diffusible activator and the indiffusible inhibitor respectively [19]; a, b, c and ε are system parameters; γ and t represent space position and time respectively; D is a diffusion coefficient and $\nabla^2=\partial^2x/\partial^2y$.

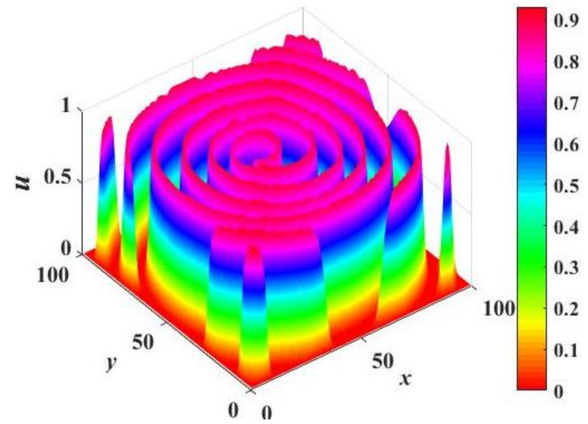

(a)

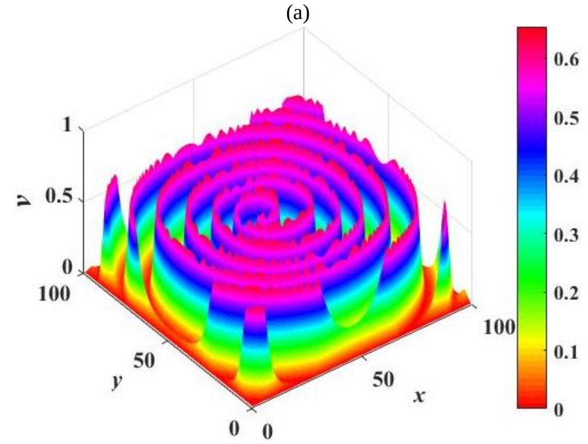

(b)

Fig. 1 The map of the spatiotemporal evolution of the state variables $u(\gamma,\ t)$ and $v(\gamma,\ t)$ at $\varepsilon=0.07$, (a) $u(\gamma,t)$, (b) $v(\gamma,t)$

The parameters are fixed as $a=0.84$, $b=0.09$, and $D=1$. Parameter ε denotes the excitability of the system. Appropriate initial conditions are selected to form a stable rotating spiral wave when $0<\varepsilon<0.06$, the spiral waves become unstable when $0.06\le\varepsilon\le0.07$, and the spiral waves breakup if the value of ε is larger than 0.07. The spatiotemporal evolution of the state variables $u(\gamma,t)$ and $v(\gamma,t)$ are given in Figs. 1 and 2 respectively, where the size of system is 100×100.

Adding bidirectional feedback to the system, and Eq. (1) is modified as Eq. (3), where d_1 and d_2 denote feedback intensity. Rewrite Eq. (3) as Eq. (4)

$$\begin{cases}\frac{\partial u(\gamma,t)}{\partial t}=\varepsilon^{-1}u(\gamma,t)\big(1-u(\gamma,t)\big)\left(u(\gamma,t)-\frac{v(\gamma,t)+b}{a}\right)\\ \qquad +D\nabla^2u(\gamma,t)-d_1u(\gamma,t)\\ \frac{\partial v(\gamma,t)}{\partial t}=f(u(\gamma,t))-v(\gamma,t)-d_2v(\gamma,t)\end{cases} \tag{3}$$

$$\begin{cases}\frac{\partial u(\gamma,t)}{\partial t}=g\big(u(\gamma,t)\big)-d_1u(\gamma,t)\\ \frac{\partial v(\gamma,t)}{\partial t}=f(v(\gamma,t))-(1+d_2)v(\gamma,t)\end{cases} \tag{4}$$

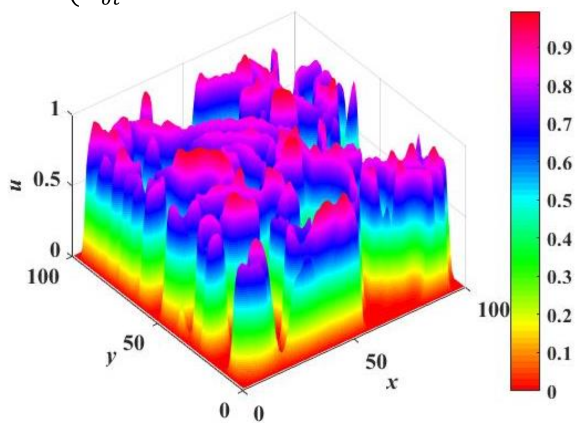

(a)

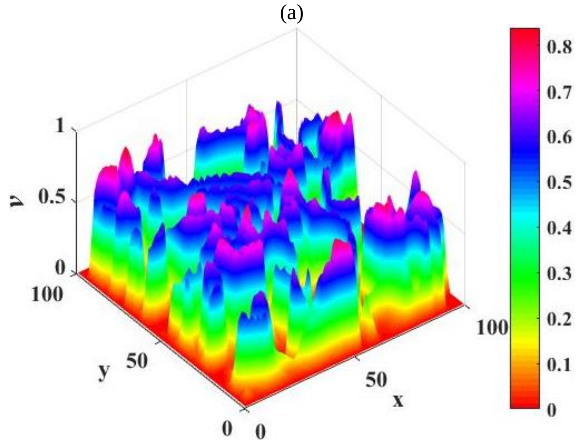

(b)

Fig. 2 The map of the spatiotemporal evolution of the state variables $u(\gamma,t)$ and $v(\gamma,t)$ at $\varepsilon=0.09$, (a) $u(\gamma,t)$, (b) $v(\gamma,t)$

where $g\big(u(\gamma,t)\big)=\frac{u(\gamma,t)}{\varepsilon}\big(1-u(\gamma,t)\big)\left(u(\gamma,t)-\frac{v(\gamma,t)+b}{a}\right)+D\nabla^2u(\gamma,t)$, τ is assumed as short time interval, and Eq. (4) is written as

$$\begin{cases}\frac{\partial u(\gamma,t+\tau)}{\partial t}=g\big(u(\gamma,t+\tau)\big)-d_1u(\gamma,t+\tau)\\ \frac{\partial v(\gamma,t+\tau)}{\partial t}=f(v(\gamma,t+\tau))-(1+d_2)v(\gamma,t+\tau)\end{cases} \tag{5}$$

Theorem 1. The system (5) will tend to stable, if feedback intensity d_1 and d_2 are taken as follows, respectively

$$\begin{cases}d_1>\xi_1\\ d_2>\xi_2-1\end{cases} \tag{6}$$

where ξ_1, ξ_2 are non-negative.

Proof: Defining the temporal variety $\Delta u(\gamma,t)$ and $\Delta v(\gamma,t)$ as

$$\begin{cases}\Delta u(\gamma,t)=u(\gamma,t+\tau)-u(\gamma,t)\\ \Delta v(\gamma,t)=v(\gamma,t+\tau)-v(\gamma,t)\end{cases}$$

The derivative form of $\Delta u(\gamma,t)$ and $\Delta v(\gamma,t)$ can be described as

$$\begin{cases}\frac{\partial\Delta u(\gamma,t)}{\partial t}=g\big(u(\gamma,t+\tau)\big)-g\big(u(\gamma,t)\big)-d_1\Delta u(\gamma,t)\\ \frac{\partial\Delta v(\gamma,t)}{\partial t}=f\big(v(\gamma,t+\tau)\big)-f\big(v(\gamma,t)\big)-(1+d_2)\Delta v(\gamma,t)\end{cases} \tag{7}$$

We establishing Lyapunov function as follow:

$$V(\gamma,t)=\frac{1}{2}\big(\Delta u(\gamma,t)^{\mathrm T}\Delta u(\gamma,t)+\Delta v(\gamma,t)^{\mathrm T}\Delta v(\gamma,t)\big)$$

The derivative form of $V(\gamma,t)$ is described as

$$\begin{aligned}\frac{\partial V(\gamma,t)}{\partial t}&=\Delta u(\gamma,t)^{\mathrm T}\frac{\partial\Delta u(\gamma,t)}{\partial t}+\Delta v(\gamma,t)^{\mathrm T}\frac{\partial\Delta v(\gamma,t)}{\partial t}\\ &=\Delta u(\gamma,t)^{\mathrm T}\big(-d_1\Delta u(\gamma,t)+\Delta g(u(\gamma,t))\big)\end{aligned}$$

$$+\Delta v(\gamma,t)^{\mathrm{T}}\big(f\big(v(\gamma,t+\tau)\big)-f\big(v(\gamma,t)\big) \\ -(1+d_2)\Delta v(\gamma,t)\big) \quad (8)$$

For two non-negative numbers ξ_1 and ξ_2, the following relationship is existed on condition of Lipschitz [33]

$$\big|g\big(u(\gamma,t+\tau)\big)-g\big(u(\gamma,t)\big)\big| \le \xi_1|u(\gamma,t+\tau)-u(\gamma,t)| \quad (9)$$

$$\big|f\big(v(\gamma,t+\tau)\big)-f\big(v(\gamma,t)\big)\big| \le \xi_2|v(\gamma,t+\tau)-v(\gamma,t)| \quad (10)$$

Substituting the adaptive law Eq. (9) and (10) into the above Eq. (8), we can obtain

$$\begin{aligned}\frac{\partial V(\gamma,t)}{\partial t} &\le \Delta u(\gamma,t)^{\mathrm{T}}\big(-d_1\Delta u(\gamma,t)+\xi_1\Delta u(\gamma,t)\big) \\ &\quad+\Big|\Delta v(\gamma,t)^{\mathrm{T}}\Big(f\big(v(\gamma,t+\tau)\big)-f\big(v(\gamma,t)\big)\Big)\Big| \\ &\quad-(1+d_2)\Delta v(\gamma,t)^{\mathrm{T}}\Delta v(\gamma,t) \\ &\le \Delta u(\gamma,t)^{\mathrm{T}}\big(-d_1\Delta u(\gamma,t)+\xi_1\Delta u(\gamma,t)\big) \\ &\quad+\Delta v(\gamma,t)^{\mathrm{T}}\big(-1-d_2\Delta v(\gamma,t)+\xi_2\Delta v(\gamma,t)\big) \\ &=(\xi_1-d_1)\Delta u(\gamma,t)^{\mathrm{T}}\Delta u(\gamma,t) \\ &\quad+(\xi_2-1-d_2)\Delta v(\gamma,t)^{\mathrm{T}}\Delta v(\gamma,t)\end{aligned}$$

Obviously, $\frac{\partial V(\gamma,t)}{\partial t}<0$ if $d_1>\xi_1$ and $d_2>\xi_2-1$. According to Lyapunov theorem, the system (5) will tend to stable.

B. Mechanism of synchronization of network constructed by Fitzhugh–Nagumo model

The N Fitzhugh–Nagumo systems are regarded as nodes of networks, where the first node is selected to control by bidirectional feedback and modified as Eq. (11), the other nodes are described as Eq. (12)

$$\begin{cases}\frac{\partial u_1(\gamma,t)}{\partial t}=g\big(u_1(\gamma,t)\big)-\eta_1\sum_{j=1}^{N}c_{1j}\,u_j(\gamma,t)-d_1u_1(\gamma,t) \\ \frac{\partial v_1(\gamma,t)}{\partial t}=f(v_1(\gamma,t))-(1+d_2)v_1(\gamma,t)\end{cases} \quad (11)$$

$$\begin{cases}\frac{\partial u_n(\gamma,t)}{\partial t}=g\big(u_n(\gamma,t)\big)-\eta_n\sum_{j=1}^{N}c_{nj}\,u_j(\gamma,t) \\ \frac{\partial v_n(\gamma,t)}{\partial t}=f(v_n(\gamma,t))-v_n(\gamma,t) \qquad (n=2,\cdots,N-1)\end{cases} \quad (12)$$

where η_i $(i=1,2,\cdots,N-1)$ denotes coupling strength, and c_{ij} is matrix element of coupling matrix C, its form is according to the class of connection, the coupled matrix is described as

$$C=\begin{bmatrix}0&0&0&\cdots&0\\-1&1&0&\cdots&0\\-1&0&1&\cdots&0\\\vdots&\vdots&\vdots&\vdots&\vdots\\-1&0&0&\cdots&1\end{bmatrix} \quad (13)$$

The errors of state variable among the network nodes are defined as

$$\begin{cases}e_{1i}(\gamma,t)=u_{i+1}(\gamma,t)-u_i(\gamma,t)\\e_{2i}(\gamma,t)=v_{i+1}(\gamma,t)-v_i(\gamma,t)\end{cases} (i=1,2,\cdots,N-1) \quad (14)$$

Firstly, the derivatives form of $e_{1i}(\gamma,t)$ and $e_{2i}(\gamma,t)$ are described as

$$\begin{cases}\dfrac{\partial e_{11}(\gamma,t)}{\partial t}=g\big(u_2(\gamma,t)\big)-\eta_2\sum_{j=1}^{N}c_{2j}u_j(\gamma,t) \\ \qquad -g\big(u_1(\gamma,t)\big)+d_1u_1(\gamma,t) \\ \dfrac{\partial e_{1n}(\gamma,t)}{\partial t}=g\big(u_{n+1}(\gamma,t)\big)-\eta_{n+1}\sum_{j=1}^{N}c_{n+1j}\,u_j(\gamma,t) \\ \qquad -g\big(u_n(\gamma,t)\big)+\eta_n\sum_{j=1}^{N}c_{nj}\,u_j(\gamma,t)\end{cases} \quad (15)$$

$$\begin{cases}\frac{\partial e_{21}(\gamma,t)}{\partial t}=f\big(v_2(\gamma,t)\big)-f\big(v_1(\gamma,t)\big)-e_{21}(\gamma,t) \\ \qquad +d_2v_1(r,t) \\ \frac{\partial e_{2n}(\gamma,t)}{\partial t}=f\big(u_{n+1}(\gamma,t)\big)-f\big(v_n(\gamma,t)\big)-e_{2n}(\gamma,t)\end{cases} \quad (16)$$

Theorem 2. If $u_1(\gamma,t)$ and $v_1(\gamma,t)$ of the first node has been stable to 0, and coupling strength of Eqs. (11) and (12) satisfies

$$\begin{cases}\eta_i>\xi_{1i}\\\eta_{n+1}\ge\eta_n\end{cases}$$

the complete synchronization of complex network can be achieved.

Proof. The Lyapunov function is constructed as

$$V(\gamma,t)=\frac{1}{2}\sum_{i=1}^{N-1}\big(e_{1i}^{\mathrm{T}}(\gamma,t)e_{1i}(\gamma,t)+e_{2i}^{\mathrm{T}}(\gamma,t)e_{2i}(\gamma,t)\big) \quad (17)$$

Based on the Eqs. (15) and (16), the derivative form of $V(\gamma,t)$ can be described as

$$\begin{aligned}\frac{\partial V(\gamma,t)}{\partial t}&=\sum_{i=1}^{N-1}e_{1i}^{\mathrm{T}}(\gamma,t)\frac{\partial e_{1i}(\gamma,t)}{\partial t}+e_{2i}^{\mathrm{T}}(\gamma,t)\frac{\partial e_{2i}(\gamma,t)}{\partial t} \\ &=e_{11}^{\mathrm{T}}(\gamma,t)\frac{\partial e_{11}(\gamma,t)}{\partial t}+\sum_{n=2}^{N-1}e_{1n}^{\mathrm{T}}(\gamma,t)\frac{\partial e_{1n}(\gamma,t)}{\partial t} \\ &\quad+e_{21}^{\mathrm{T}}(\gamma,t)\frac{\partial e_{21}(\gamma,t)}{\partial t}+\sum_{n=2}^{N-1}e_{2n}^{\mathrm{T}}(\gamma,t)\frac{\partial e_{2n}(\gamma,t)}{\partial t} \\ &=e_{11}^{\mathrm{T}}(\gamma,t)\Bigg(g\big(u_2(\gamma,t)\big)-\eta_2\sum_{j=1}^{N}c_{2j}\,u_j(\gamma,t) \\ &\quad-g\big(u_1(\gamma,t)\big)+d_1u_1(\gamma,t)+\eta_1\sum_{j=1}^{N}c_{1j}\,u_j(\gamma,t)\Bigg) \\ &\quad+\sum_{n=2}^{N-1}e_{1n}^{\mathrm{T}}(\gamma,t)\Bigg(-\eta_{n+1}\sum_{j=1}^{N}c_{n+1j}\,u_j(\gamma,t) \\ &\quad+g\big(u_{n+1}(\gamma,t)\big)-g\big(u_n(\gamma,t)\big) \\ &\quad+\eta_n\sum_{j=1}^{N}c_{nj}\,u_j(\gamma,t)\Bigg)+e_{21}^{\mathrm{T}}(\gamma,t)\big(f\big(v_2(\gamma,t)\big) \\ &\quad-f\big(v_1(\gamma,t)\big)-e_{21}(\gamma,t)+d_2v_1(\gamma,t)\big) \\ &\quad+\sum_{n=2}^{N-1}e_{2n}^{\mathrm{T}}(\gamma,t)\big(f\big(v_{n+1}(\gamma,t)\big)-f\big(v_n(\gamma,t)\big) \\ &\quad-e_{2n}(r,t)\big)\end{aligned} \quad (18)$$

According to the form of coupling matrix C, Eq. (18) can be simplified as:

$$\begin{aligned}\frac{\partial V(\gamma,t)}{\partial t}&=e_{11}^{\mathrm{T}}(\gamma,t)\big(g\big(u_2(\gamma,t)\big)-g\big(u_1(\gamma,t)\big)-\eta_2e_{11}(\gamma,t) \\ &\quad+d_1u_1(\gamma,t)\big)+\sum_{n=2}^{N-1}e_{1n}^{\mathrm{T}}(\gamma,t)\big[g\big(u_{n+1}(\gamma,t)\big) \\ &\quad-g\big(u_n(\gamma,t)\big)-\eta_{n+1}\big(u_{n+1}(\gamma,t)-u_1(\gamma,t)\big) \\ &\quad+\eta_n\big(u_n(\gamma,t)-u_1(\gamma,t)\big)\big]+e_{21}^{\mathrm{T}}(\gamma,t)\big(f\big(v_2(\gamma,t)\big) \\ &\quad-f\big(v_1(\gamma,t)\big)-e_{21}(\gamma,t)+d_2v_1(\gamma,t)\big) \\ &\quad+\sum_{n=2}^{N-1}e_{2n}^{\mathrm{T}}(\gamma,t)\big(f\big(u_{n+1}(\gamma,t)\big)-f\big(v_n(\gamma,t)\big) \\ &\quad-e_{2n}(\gamma,t)\big)\end{aligned} \quad (19)$$

For non-negative numbers ξ_{1n} and ξ_{2n}, the following relationships are existed on condition of Lipschitz

$$|g(u_{n+1}(\gamma,t)) - g(u_n(\gamma,t))| \le \xi_{1n}|u_{n+1}(\gamma,t) - u_n(\gamma,t)| \tag{20}$$

$$|f(v_{n+1}(\gamma,t)) - f(v_n(\gamma,t))| \le \xi_{2n}|v_{n+1}(\gamma,t) - v_n(\gamma,t)| \tag{21}$$

Substituting the Eqs. (20) and (21) into the Eq. (19), we can get

$$\begin{aligned}\frac{\partial V(\gamma,t)}{\partial t} \le & \sum_{i=1}^{N-1}(\xi_{1i} - \eta_{i+1})e_{1i}^{\mathrm{T}}(\gamma,t)e_{1i}(\gamma,t) \\ & + e_{11}^{\mathrm{T}}(\gamma,t)d_1u_1(\gamma,t) \\ & + \sum_{n=2}^{N-1}(\eta_n - \eta_{n+1})(u_n(\gamma,t) + u_1(\gamma,t)) \\ & + \sum_{i=1}^{N-1}(\xi_{2i} - 1)e_{2i}^{\mathrm{T}}(\gamma,t)e_{2i}(\gamma,t) \\ & + e_{21}^{\mathrm{T}}(\gamma,t)d_2v_1(\gamma,t)\end{aligned} \tag{22}$$

When the wave and turbulence of the first node is cancelled, we can obtain $u_1(\gamma,t) = 0$ and $v_1(\gamma,t) = 0$, and the Eq. (22) is simplified as:

$$\begin{aligned}\frac{\partial V(\gamma,t)}{\partial t} \le & \sum_{i=1}^{N-1}(\xi_{1i} - \eta_{i+1})e_{1i}^{\mathrm{T}}(\gamma,t)e_{1i}(\gamma,t) \\ & + \sum_{i=1}^{N-1}(\xi_{2i} - 1)e_{2i}^{\mathrm{T}}(\gamma,t)e_{2i}(\gamma,t) \\ & + \sum_{n=2}^{N-1}(\eta_n - \eta_{n+1})(u_n(\gamma,t) + u_1(\gamma,t))\end{aligned}$$

where ξ_{2i} is fixed as $\xi_{2i} < 1$. As Fig. 1 shows, $u_n(\gamma,t) \in [0,1]$, it is obvious that, if coupling strength satisfies $\eta_{i+1} > \xi_{1i}$ and $\eta_{n+1} \ge \eta_n$, there will be $\frac{\partial V(\gamma,t)}{\partial t} < 0$. Based on the Lyapunov theorem, the synchronization of network has been achieved, and spiral waves or the spatiotemporal chaos of the other $N-1$ nodes will be cancelled. That completes the proof.

III. Math Numerical Simulation

A. Example 1

In the numerical simulation, parameters d_1 and d_2 are fixed as $d_1 = 1.7$ $d_2 = 2$, $\tau = 5$, $\xi_m = 0.01$ $(m = 1,2,3)$, the number of the nodes is designed as $N = 3$, bidirectional feedback is added at $t = 50$, where $L = 100$ is the size of system.

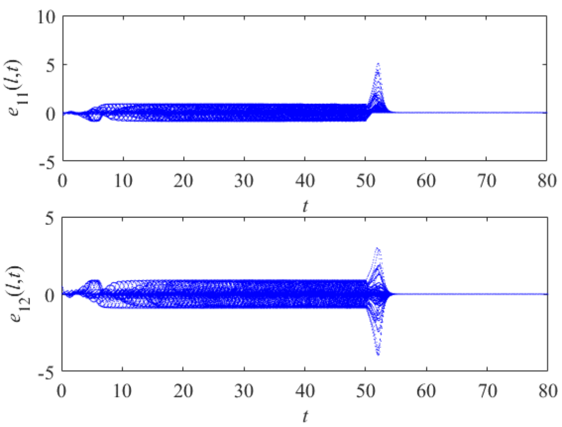

(a)

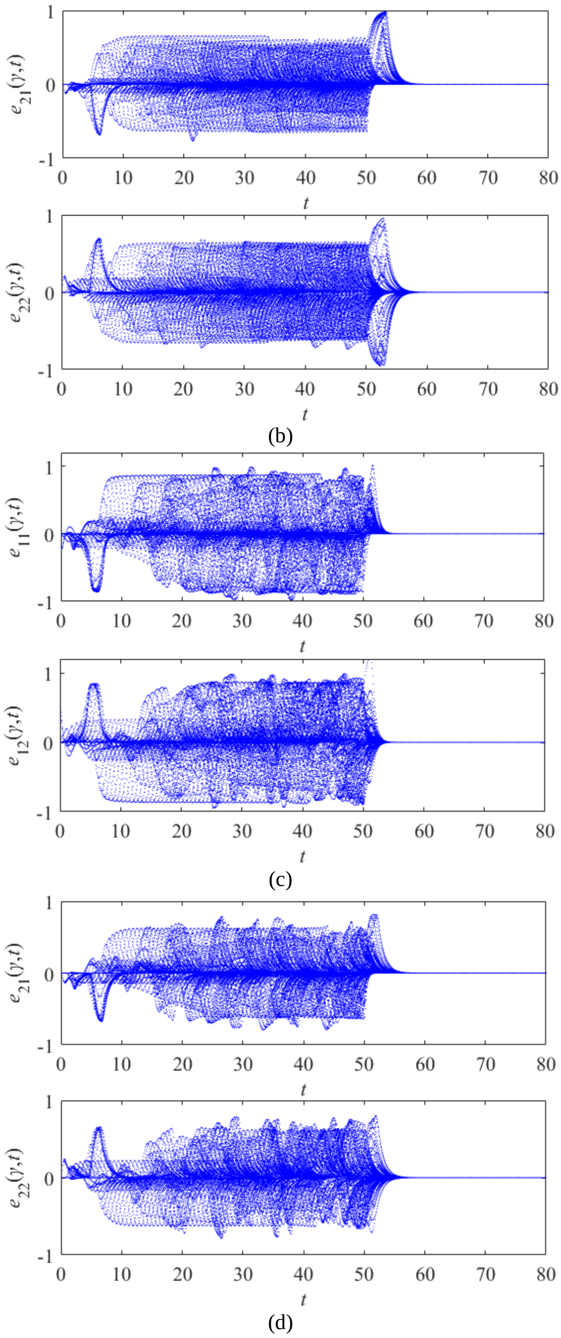

Fig.3 Temporal evolution of errors $e_{1i}(\gamma,t)$ and $e_{2i}(\gamma,t)$ $(i = 1,2)$, (a) (b) $\varepsilon = 0.07$; (c) (d) $\varepsilon = 0.09$ $(\gamma = 43)$

Inputting bidirectional feedback and couplings at $t = 50$, the spatial evolution of network errors $e_{1i}(\gamma,t)$ and $e_{2i}(\gamma,t)$, $(i = 1, 2)$ are shown in Fig. 3, the initial temporal evolution of errors changed markedly, because the initial values is different, then errors toward zero rapidly with the synchronization of the network.

Process of elimination of $u_1(\gamma,t)$, $u_2(\gamma,t)$ and $u_3(\gamma,t)$ are shown in Fig. 4 and Fig. 5, if values of the $u_1(\gamma,t)$, $u_2(\gamma,t)$ and $u_3(\gamma,t)$ are stable to 0, the spiral waves or spatiotemporal chaos of network are cancelled.

In order to describe the elimination process of spiral waves and spatiotemporal chaos, ΔU_i and ΔV_i are defined as

$$\begin{cases} \Delta U_i = \oiint_{D_{xy}} \sqrt{\frac{1}{L^2}\Delta {u_i}^2 dxdy} \\ \Delta V_i = \oiint_{D_{xy}} \sqrt{\frac{1}{L^2}\Delta {v_i}^2 dxdy} \end{cases} \quad (i = 1, \cdots N) \quad (23)$$

As shown in Figs. 6 and 7, the variables of system change quickly from $t = 0$ to $t = 40$, then the variables of system fluctuate slightly, when we add bidirectional feedback to the network at $t = 50$, the variables are eliminated very quickly, it is obvious that spiral waves and turbulence of Fitzhugh–Nagumo model are eliminated effectively and quickly.

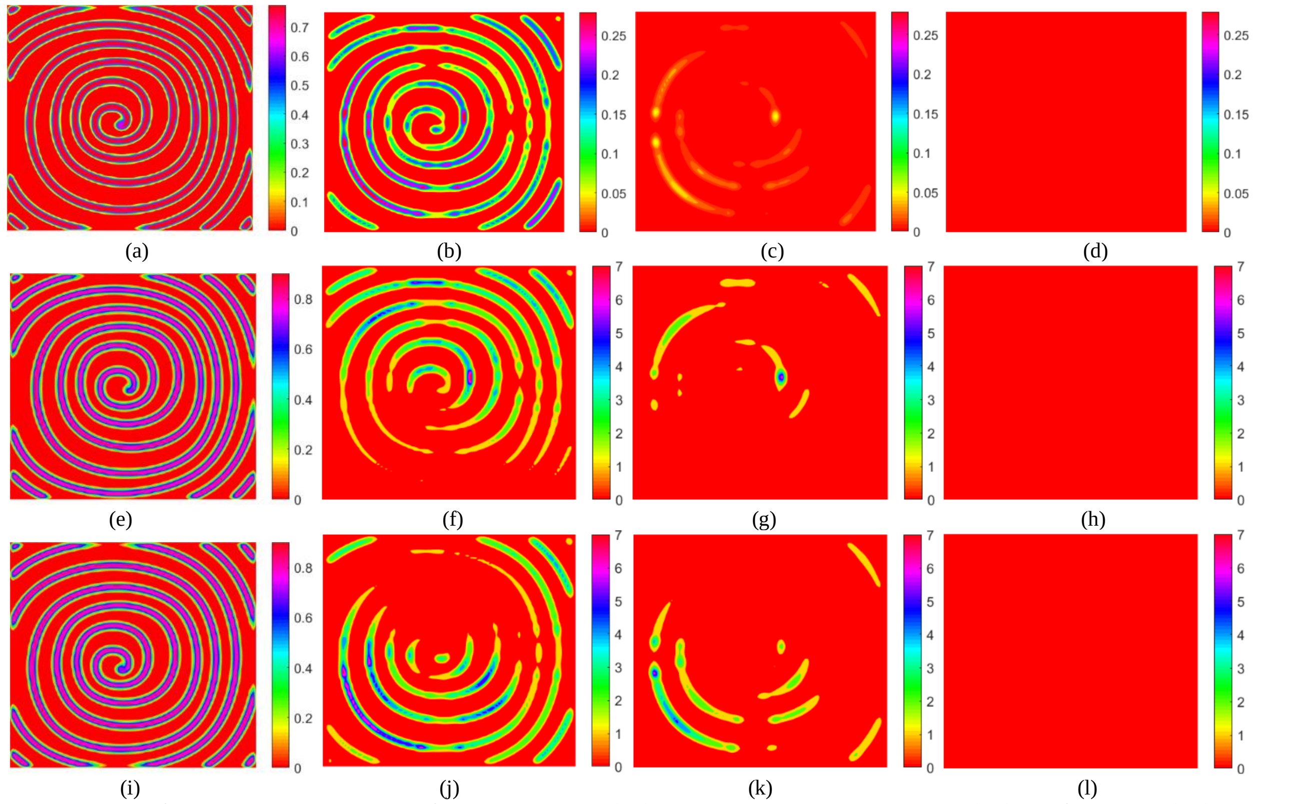

Fig. 4 Projection map of the spatiotemporal evolution of the state variable $u_i(r,t)$ at $\varepsilon = 0.07$, where (a) (b) (c) (d): $u_1(\gamma,t)$; (e) (f) (g) (h): $u_2(\gamma,t)$; (i) (j) (k) (l): $u_3(\gamma,t)$, and (a) (e) (i): $t = 50$; (b) (f) (j): $t = 52$; (c) (g) (k): $t = 53$; (d) (h) (l): $t = 55$

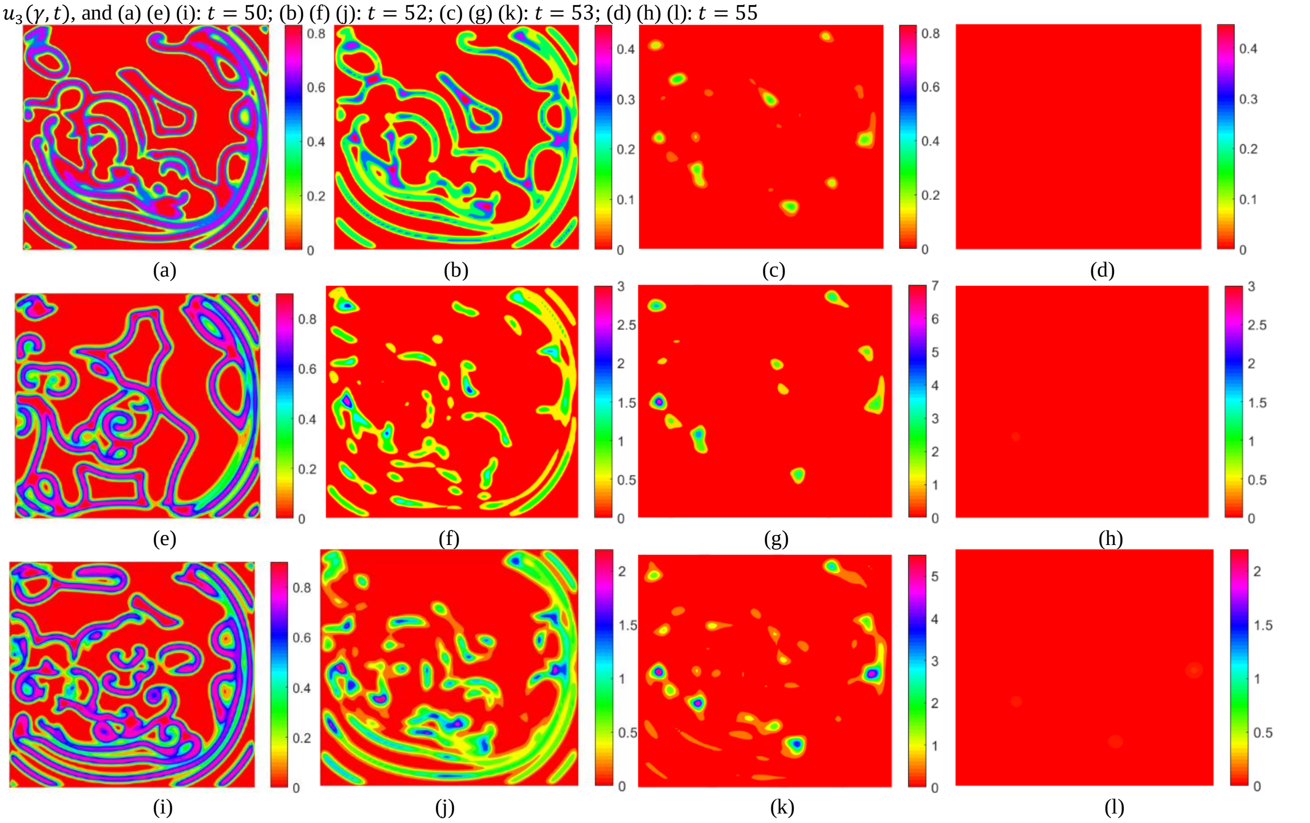

Fig. 5 Projection map of the spatiotemporal evolution of the state variable $u_i(r,t)$ at $\varepsilon = 0.09$, where (a) (b) (c) (d): $u_1(\gamma,t)$; (e) (f) (g) (h): $u_2(\gamma,t)$; (i) (j) (k) (l): $u_3(\gamma,t)$, and (a) (e) (i): $t = 50$; (b) (f) (j): $t = 51$; (c) (g) (k): $t = 52$; (d) (h) (l): $t = 55$

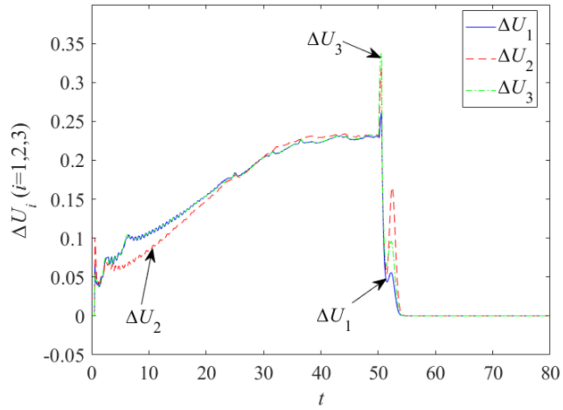

(a)

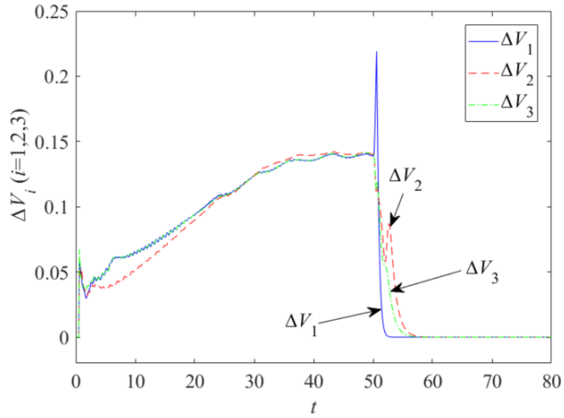

(b)

Fig. 6 Temporal evolution of ΔU_i, and ΔV_i, where $\varepsilon = 0.07$, $\eta_2 = 2$, $\eta_3 = 4$, (a) ΔU_i, (b) ΔV_i

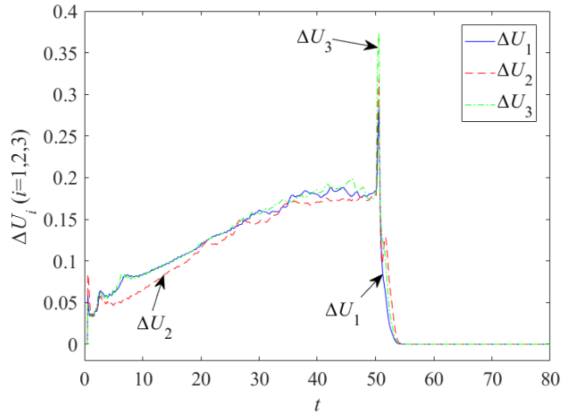

(a)

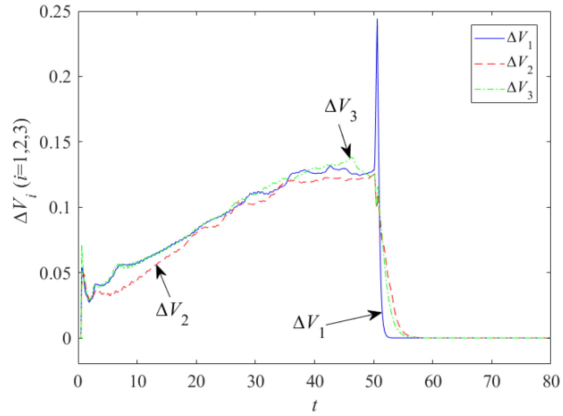

(b)

Fig. 7 Temporal evolution of ΔU_i, and ΔV_i, where $\varepsilon = 0.09$, $\eta_2 = 2$, $\eta_3 = 4$, (a) ΔU_i, (b) ΔV_i

B. Example 2

In order to further validate the feasibility and effectiveness of the proposed method, the number of nodes is expended to 30. Fig. 8 shows the temporal evolution of e_i $(i = 1, 2, \cdots, 29)$ at the place $x = 45$ and $y = 43$. Fig. 9 exhibits the development of ΔU_i. Based on Figs. 8 and 9, it is found that performance of the synchronization and effectiveness of elimination are insensitive to the scale of network.

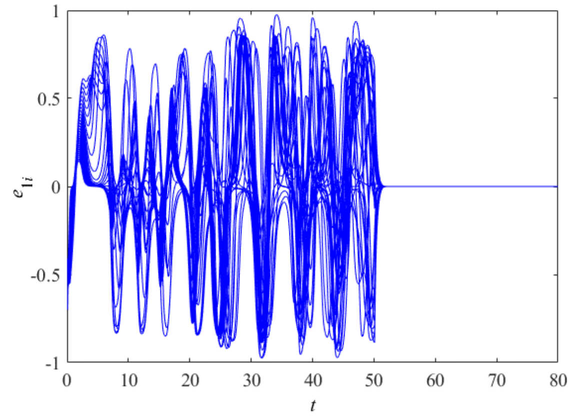

(a)

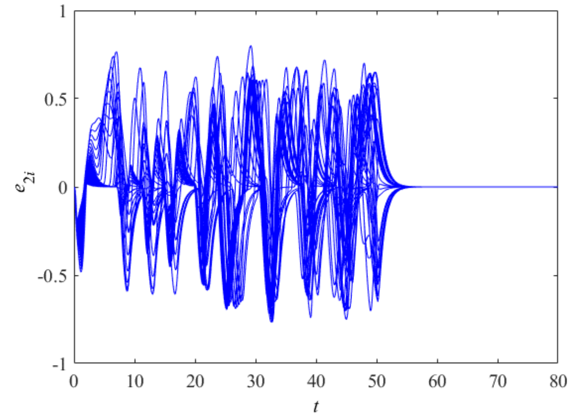

(b)

Fig.8 Temporal evolution of error e_{1i}, e_{2i} where $\varepsilon = 0.09$, $\eta_i = 1.7$, $i = 1,2,\cdots,29$ $(x = 45, y = 43)$, (a) e_{1i}, (b) e_{2i}

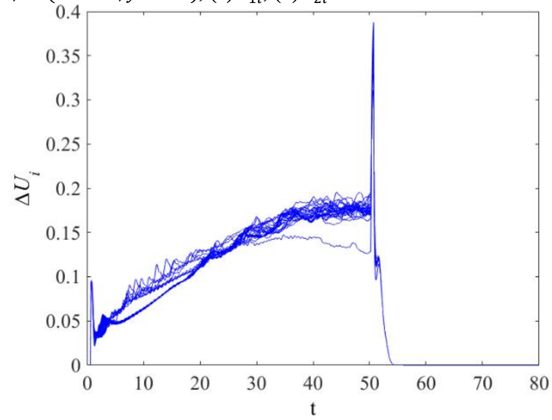

Fig.9 Temporal evolution of ΔU_i, where $\varepsilon = 0.09$, $\eta_i = 1.7$, $i = 1,2,\cdots,30$

IV. Analysis and Discussion

In this section, the proposed synchronization method is compared with previous synchronization method.

A. Synchronization based on active-passive decomposition (APD) method

Eqs. (11) and (12) are rewritten as

$$\begin{cases} \frac{\partial u_1'}{\partial t} = \varepsilon^{-1} u_1'(1-u_1')\left(u_1' - \frac{v_1'+b}{a}\right) + D\nabla^2 u_1' - \sum_{j=1}^{N} c_{1j} S_j - d_1 u_1' \\ \frac{\partial v_1'}{\partial t} = f(u_1') - v_1' - d_2 v_1' \end{cases} \tag{24}$$

$$\begin{cases} \frac{\partial u_i'}{\partial t} = \varepsilon^{-1} u_i'(1-u_i')\left(u_i' - \frac{v_i'+b}{a}\right) + D\nabla^2 u_i' - \sum_{j=1}^{N} c_{ij} S_j \\ \frac{\partial v_i'}{\partial t} = f(u_i') - v_i' \quad (n = i, \cdots, N-1) \end{cases} \tag{25}$$

where

$$f(u_i') = \begin{cases} 0 & 0 \le u_i' < 1/3 \\ 1 - c u_i'(u_i'-1)^2 & 1/3 \le u_i' < 1 \\ 1 & u_i' \ge 1 \end{cases}$$

$$S_j = \frac{u_j'}{\varepsilon}\left(u_j' - \frac{v_j'}{a} - u_j'^2 + \frac{u_j' v_j'}{a} - \frac{b}{a} u_j'\right)$$

S_j is driven signal, the coupled matrix is described as Eq. (13), and errors of state variable among the network nodes are defined as

$$\begin{cases} e_{1i}' = u_i' - u_{i+1}' \\ e_{2i}' = v_i' - v_{i+1}' \quad (i = 1,2,\cdots,N-1) \end{cases} \tag{26}$$

B. Synchronization based on Lyapunov exponent method

We rewrite Eqs. (11) and (12) as

$$\begin{cases} \frac{\partial u_1''}{\partial t} = \varepsilon^{-1} u_1''(1-u_1'')\left(u_1'' - \frac{v_1''+b}{a}\right) + D\nabla^2 u_1'' - k\sum_{j=1}^{N} c_{1j} u''_j \\ \qquad -d_1 u_1'' \\ \frac{\partial v_1''}{\partial t} = f(u_1'') - v_1'' - d_2 v_1'' \quad (n = 2, \cdots, N-1) \end{cases} \tag{27}$$

$$\begin{cases} \frac{\partial u_n''}{\partial t} = \varepsilon^{-1} u_n''(1-u_n'')\left(u_n'' - \frac{v_n''+b}{a}\right) + D\nabla^2 u_n'' + k(u_1'' - u_n'') \\ \frac{\partial v_n''}{\partial t} = f(u_n'') - v_n'' \quad (n = 2, \cdots, N-1) \end{cases} \tag{28}$$

where

$$f(u_i'') = \begin{cases} 0 & 0 \le u_i'' < 1/3 \\ 1 - c u_i''(u_i''-1)^2 & 1/3 \le u_i'' < 1 \\ 1 & u_i'' \ge 1 \end{cases}$$

k is coupling strength between the nodes of network, the coupled matrix is assumed as Eq. (13), and errors of state variable among the network nodes are defined as

$$\begin{cases} e_{1i}'' = u_i'' - u_{i+1}'' \\ e_{2i}'' = v_i' - v_{i+1}'' \quad (i = 1,2,\cdots,N-1) \end{cases} \tag{29}$$

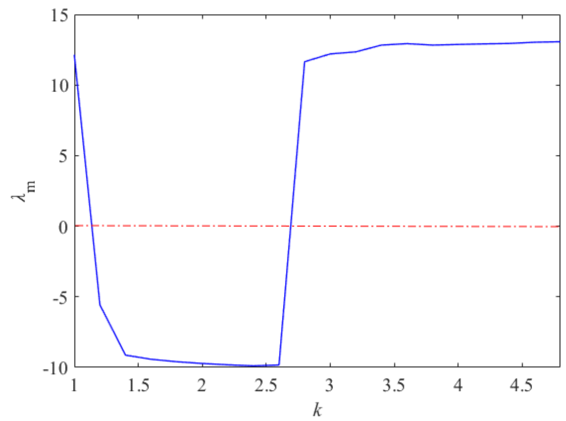

Fig.10 The evolution of maximum Lyapunov exponent with parameter k

Fitzhugh–Nagumo models are assigned with different initial values, and the evolution of maximum Lyapunov exponent λ_m of Eq. (29) with the coupling strength k is shown in Fig. 10. When the maximum Lyapunov exponent is negative, the synchronization of network is achieved. The negative maximum Lyapunov exponent is smaller, the network approaches to synchronization at the faster the speed. As Fig. 10 demonstrates, Lyapunov exponent is minimum, when $k = 2.3$.

C. Comparison and analysis

In order to compare the synchronization performance of our proposed method with APD and Lyapunov exponent methods, we define global errors as

$$\begin{cases} E_1 = \frac{1}{N-1}\sum_{i=1}^{N-1} \lim_{t\to\infty} \oiint_{D_{xy}} \sqrt{\frac{1}{L^2} e_{1i} dxdy} \\ E_2 = \frac{1}{N-1}\sum_{i=1}^{N-1} \lim_{t\to\infty} \oiint_{D_{xy}} \sqrt{\frac{1}{L^2} e_{2i} dxdy} \end{cases} \tag{30}$$

$$\begin{cases} E_1' = \frac{1}{N-1}\sum_{i=1}^{N-1} \lim_{t\to\infty} \oiint_{D_{xy}} \sqrt{\frac{1}{L^2} e_{1i}' dxdy} \\ E_2' = \frac{1}{N-1}\sum_{i=1}^{N-1} \lim_{t\to\infty} \oiint_{D_{xy}} \sqrt{\frac{1}{L^2} e_{2i}' dxdy} \end{cases} \tag{31}$$

$$\begin{cases} E_1'' = \frac{1}{N-1}\sum_{i=1}^{N-1} \lim_{t\to\infty} \oiint_{D_{xy}} \sqrt{\frac{1}{L^2} e_{1i}'' dxdy} \\ E_2'' = \frac{1}{N-1}\sum_{i=1}^{N-1} \lim_{t\to\infty} \oiint_{D_{xy}} \sqrt{\frac{1}{L^2} e_{2i}'' dxdy} \end{cases} \tag{32}$$

where E_1 and E_2 are global errors of Eqs. (11) and (12), E_1' and E_2' are global errors of Eqs. (24) and (25), E_1'' and E_2'' are global errors of Eqs. (27) and (28).

As Fig. 11 shows, global errors based on our method and Lyapunov exponent method approach to zero more quickly than APD method, and global errors based on our method approach to zero at the best speed of Lyapunov exponent method.

V. CONCLUSION

Elimination of spiral waves or spatiotemporal chaos based on synchronization of network is investigated in this paper. N Fitzhugh–Nagumo models are taken as nodes of network, when a single node is eliminated, spiral waves and turbulence of the other nodes are canceled through synchronization of network. Two Numerical simulation results show that proposed method can be successfully used to achieve the synchronization and to eliminate spiral waves or spatiotemporal chaos, furthermore, the scale of the network does not affect the synchronization performance. In addition, our proposed method has better synchronization performance than APD and Lyapunov exponent methods.

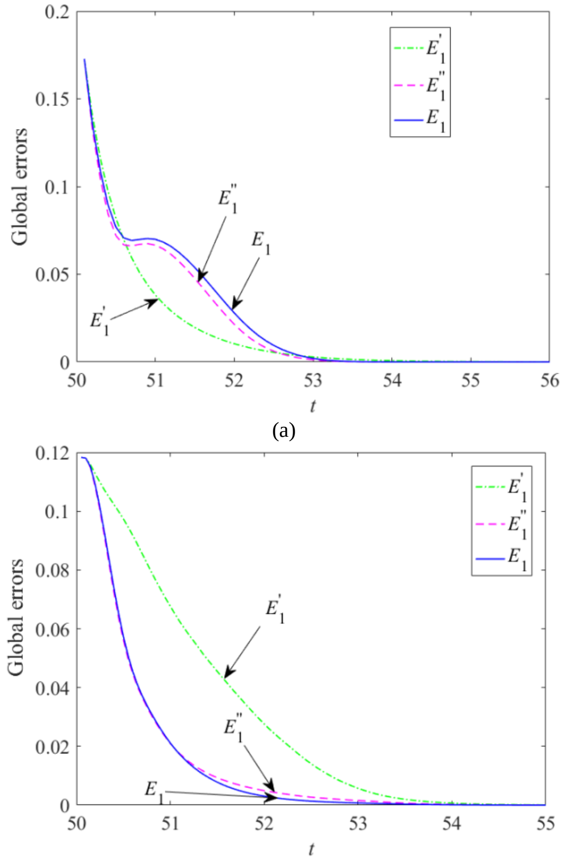

(a)
(b)

Fig.11 The evolution of global errors, where $k = 2.3$, $\eta_n = 2 + 0.01(n-1)$, $n = 2,3,\cdots,30$, (a) $\varepsilon = 0.07$, (b) $\varepsilon = 0.09$

REFERENCES

[1] Pal S, Petrovskii S, Ghorai S, "Spatiotemporal pattern formation in 2D prey-predator system with nonlocal intraspecific competition," Communications in Nonlinear Science and Numerical Simulation, vol. 93, 2021.

[2] Dezfoli ARA, Lin SK, Hsu WD, "Simulations of domain pattern in lead-titanate by molecular dynamics simulations aided q-state Potts model," Computational Materials Science, vol. 110, pp. 221-226, 2015.

[3] Castelino JK, Ratliff DJ, Rucklidge AM, "Spatiotemporal chaos and quasipatterns in coupled reaction-diffusion systems," Physica D-Nonlinear Phenomena, vol. 409, 2020.

[4] Ziani Z, Leveque G, Akjouj A, "Characterization of spatiotemporal chaos in arrays of nonlinear plasmonic nanoparticles," Physical Review B, vol. 100, no. 16, 2019.

[5] Jamet Q, Dewar WK, Wienders N, "Spatiotemporal patterns of chaos in the Atlantic overturning circulation," Geophysical Research Letters, vol. 46, no. 13, pp. 7509-7517, 2019.

[6] Xie BL, "Pattern dynamics in a vegetation model with time delay," Physica a-Statistical Mechanics and Its Applications, vol. 443, pp. 460-466, 2016.

[7] Zhang J, Yan G, Wan M, "Lattice Boltzmann simulations for the vortex tori pattern in the three-dimensional cubic-quintic complex Ginzburg-Landau equation," Journal of Computational Physics, vol. 306, pp. 311-319, 2016.

[8] Huang ZJ, Li QY, Bai J, "Entropy measurement of ordered patterns in neuronal network with repulsive coupling," ACTA Physica Sinica, vol. 68, no. 11, 2019.

[9] Shepelev IA, Muni SS, Vadivasova TE, "Spatiotemporal patterns in a 2D lattice with linear repulsive and nonlinear attractive coupling," Chaos, vol. 31, no. 4, 2021.

[10] Gomes JM, Lobosco M, dos Santos RW, "Delay differential equation-based models of cardiac tissue: Efficient implementation and effects on spiral-wave dynamics," Caos, vol. 29, no. 12, 2019.

[11] Li QY, Huang ZJ, Tang GN, "Eliminating spiral wave and spatiotemporal chaos in cardiac tissues by eliminateing the rotation of spiral wave tip," ACTA Physica Sinica, vol. 67, no. 24, 2018.

[12] Feng X, Gao X, Tang J, "Wave trains induced by circularly polarized electric fields in cardiac tissues," Scientific Reports, vol. 5, 2015.

[13] Hoffman MJ, LaVigne NS, Scorse ST, "Reconstructing three-dimensional reentrant cardiac electrical wave dynamics using data assimilation," Chaos, vol. 26, no. 1, 2016.

[14] Kharche SR, Biktasheva IV, Seemann G, "A computer simulation study of Anatomy induced drift of spiral waves in the human Atrium," Biomed Research International, 2015.

[15] Marcotte CD, Grigoriev RO, "Unstable spiral waves and local Euclidean symmetry in a model of cardiac tissue,". Chaos, vol. 25, no. 6, 2015.

[16] Nakouzi E, Tot JF, Zhang ZH, "Hysteresis and drift of spiral waves near heterogeneities: From chemical experiments to cardiac simulations," Physical Review E, vol. 93, no. 2, 2016.

[17] Nash MP, Panfilov AV, "Electromechanical model of excitable tissue to study reentrant cardiac arrhythmias," Progress in Biophysics & Molecular Biology, vol. 85, no. 2-3, pp. 501-522, 2004.

[18] Horning M, "Termination of pinned vortices by high-frequency wave trains in heartlike excitable media with anisotropic fiber orientation," Physical Review E, vol.86, no. 3, 2012.

[19] Otani NF, "Termination of reentrant cardiac action potential propagation using far-field electrical pacing," IEEE Transactions on Biomedical Engineering, vol. 58, no. 7, pp. 2013-2022, 2011.

[20] Pan DB, Gao X, Feng X, "Removal of pinned scroll waves in cardiac tissues by electric fields in a generic model of three-dimensional excitable media," Scientific Reports, vol. 6, 2016.

[21] Shajahan TK, Krinski VI, Knyazeva S, "Eliminating Pinned Spiral Waves in Cardiac Monolayer by Far Field Pacing," 2014 8th Conference of the European Study Group on Cardiovascular Oscillations.

[22] Zhou ZW, Wang LL, Qiao CG, "Terminating spiral waves and spatiotemporal chaos in heart by synchronous repolarization," ACTA Physica Sinica, vol. 62, no. 15, 2013.

[23] Li QY, Bai J, Tang GN, "Control of spiral wave and spatiotemporal chaos in two-layer aging cardiac tissues," ACTA Physica Sinica, vol. 70, no. 9, 2021.

[24] Luo HB, Ma JL, "Dynamic behaviors of spiral waves in cardiac tissue under electromagnetic radiation," AIP Advances, vol. 10, no. 5, 2020.

[25] Xu B, Jacquir S, Laurent G, "A hybrid stimulation strategy for elimination of spiral waves in cardiac tissue," Chaos Solitons & Fractals, vol. 44, no. 8, pp. 633-639, 2011.

[26] Guo W, Qiao C, Zhang Z, "Spontaneous elimination of spiral turbulence based on feedback strategy," Physical Review E, vol. 81, no. 5, 2010.

[27] Yuan GY, Wang XM, Wang GR, "Effect of External periodic pulses on spiral dynamics and control of spiral waves," International Journal of Modern Physics B, vol. 27, no. 28, 2013.

[28] Jia LS, Zhao R, Pan W, "Controlling spiral waves and spatiotemporal chaos by dislocation coupling," 2015 11th International Conference on Natural Computation, pp. 545-549.

[29] Lu L,. Ge LJ, Gao LY, "Synchronization transmission of spiral wave and turbulence in uncertain time-delay neuronal networks," Physica a-Statistical Mechanics and its Applications," vol. 525, pp. 64-71, 2019.

[30] Lu L, Li CR, Li G, "Synchronization transmission of spiral wave and turbulence within the uncertain switching network," Physica a-Statistical Mechanics and its Applications," vol. 474, pp. 85-98, 2017.

[31] Zhang QL, Lu L, Zhang Y, "Elimination of spiral waves and spatiotemporal chaos by the synchronization transmission technology of network signals," Chinese Physics B," vol. 20, no. 1, 2011.

[32] Hildebrand M, Bar M, Eiswirth M, "Statistics of topological defects and spatiotemporal chaos in a reaction-diffusion system," Physical Review Letters, vol. 78, no. 5, pp. 1503-1506, 1995.

[33] Li CR, Lu L, Yang YM, "Research on outer synchronization between uncertain time-varying networks with different node number," Physica a-Statistical Mechanics and its Applications, vol. 492, pp. 2301–2309, 2018.